# Length scales and alloys of iron

IOP Conf. Series: Materials Science and Engineering **580** (2019) 012002 doi:10.1088/1757-899X/580/1/012002

# Length scales and alloys of iron

**H K D H Bhadeshia**

University of Cambridge, Materials Science and Metallurgy, CB3 0FS, UK

E-mail: hkdb@cam.ac.uk

**Abstract.** Many of the structures common within steels are not geometrically smooth, which means that their stereological parameters, such as the amount of interfacial area per unit volume, are resolution dependent. The tendency of brittle phases to crack is size dependent, as is the strength. The ability of steel to resist cleavage can be influenced by the size and distribution of coherent domains within the structure. A different diffusion theory applies when dealing with steep concentration gradients. All of these aspects are of importance in the design, characterisation and theory of steels, illustrated here with a few examples, where the neglect of length scales is improper.

## 1. Introduction

We do not as yet attach sufficient significance to length scales in the context of engineering materials. The problem is compounded by the plethora of characterisation methods and theoretical treatments, that cover many orders of magnitude of resolution. The purpose of the work presented here is to describe a few phenomena related to steels, where neglect of the coupling between length scale and theory or experiment, can become problematic.

## 2. Rough objects

It is intriguing that platelets of bainite ($\alpha_b$) are arrested in their growth before they encounter a hard obstacle, such as an austenite grain boundary [1]. There is a shape deformation [2, 3], too large to accommodate elastically in the temperature regime where bainite grows. This causes the adjacent austenite to relax by plastic deformation [4, 5], creating a large density of tangled dislocations in the vicinity of the transformation interface [6]. This blocks the motion of the glissile $\alpha_b/\gamma$ interface [7], causing *mechanical stabilisation* [8, 9]. The platelets therefore grow to a limited size, so the transformation must propagate by the formation of new platelets, each of a limited size. The best location for a new platelet to form is either at the austenite grain boundary or at the tip of a prior platelet. Both of these sites activate to generate clusters of platelets that are known as sheaves.

The structure of a sheaf is illustrated in figure 1 at a variety of resolutions. Platelets of bainitic ferrite are separated by films of retained austenite ($\gamma$). These platelets are in fact contiguous and hence in the same crystallographic orientation in space. This means that the shape of the austenite/ferrite interface is complex, making any attempt to determine the amount of interface per unit volume ($S_V$) dependent on the spatial resolution of the measurement technique used.

In the terminology of fractal dimensions, the interface is said to be *rough*. This contrasts with smooth objects whose stereological properties do not depend on resolution. A perfect circle would have a precise perimeter, a perfect sphere an exact surface area, both quantities

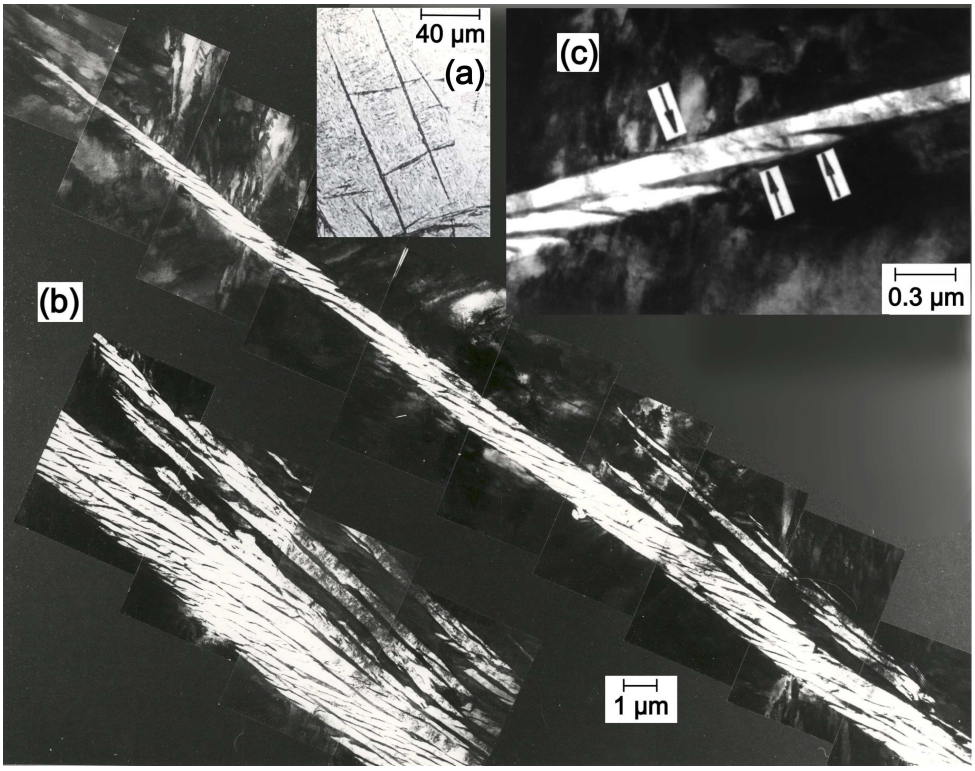


**Figure 1.** Structure of a bainite sheaf at a variety of resolutions [10]. (a) Optical micrograph, the dark plate-like features are bainite sheaves. (b) Transmission electron micrograph montage showing detailed structure of sheaf, consisting of very many platelets, each about 10 μm in length. (c) Another generation of much shorter sub-critical platelets.

defined by explicit equations independent of resolution. There is a theory for roughness [11], in which a fractal dimension $D$ determines how, for example, the perimeter of a rough object such as the outline map of Scotland, scales with resolution. The dimension can be determined from the gradient of a plot of $\ln N_i$ against $\ln \varepsilon_i^{-1}$, where $i = 1, 2, 3, \ldots$ is the number of different resolutions at which measurements are made, $N_i \times \varepsilon_i$ is the total length measured at a particular resolution $\varepsilon_i$.

In the case of bainite, the $\alpha_b/\gamma$ interfacial area per unit volume is an important parameter in determining a variety of properties, such as toughness, the ability to trap hydrogen [12] etc. [13].

Toughness is related to the size of the plastic zone at a crack tip [14], so the appropriate resolution for a typical steel would be of the order of 10 μm, whereas the scale is much smaller when it comes to hydrogen absorption at an interface. It would not be unreasonable in the latter case to measure $S_V$ with a resolution that is close to atomic, since there are multiple interstices per iron atom where hydrogen can reside [15]. The interfacial area per unit volume is given by:

$$\ln S_v = S_\circ \varepsilon^{(D_T - D)}, \tag{1}$$

where $S_\circ$ is the surface to volume ratio of a smooth object with a topological dimension $D_T$, and $D$ is the fractal dimension. By measuring $S_V$ at a variety of resolutions, the fractal dimension for the bainite-austenite interfacial area has been determined as follows:

$$\ln S_V = 0.59 \ln \varepsilon^{-1} + 5.4 \tag{2}$$


**Figure 2.** Measuring the perimeter of Scotland with callipers, set to a resolution ε. The nooks and crannies are not captured at the resolution illustrated, but the finer features would enlarge the perimeter if the distance ε between its ends is reduced.

where 0.59 is the slope of the line in figure 3, i.e., $D - D_{\mathrm{T}}$, with $D_{\mathrm{T}} = 3$ for the three-dimensional object that a bainite sheaf is. Using this, it is possible to calculate the amount of surface per unit volume as a function of resolution, and the information used in order to address particular properties. It is emphasised however, that the bainite sheaf is not in fact a true fractal object because the self-similarity of platelets does not extend to indefinitely finer scales. So the change in $S_{\mathrm{V}}$ with resolution is smaller than if the structure represented a true fractal.

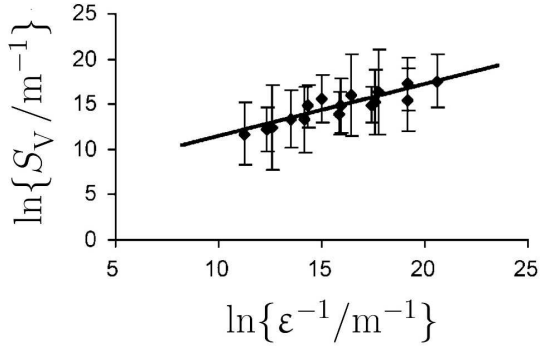


(a)

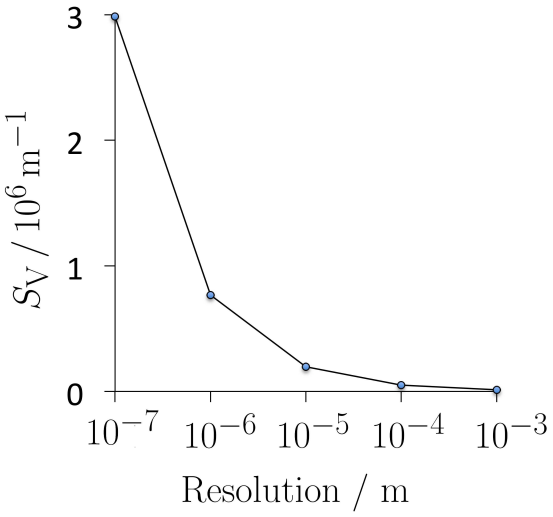


(b)

**Figure 3.** (a) Plot to determine the fractal dimension of $\alpha_{\mathrm{b}}/\gamma$ interfaces; (b) variation in $S_{\mathrm{V}}$ as a function of resolution [16].

## 3. Cracking and complexity

It has been possible to create the largest ever density of strong-interfaces, some 100 million $\mathrm{m}^2/\mathrm{m}^3$, in steel by heat treatment alone [17–19]. The structure consists of platelets of bainitic ferrite, just 20-40 nm in thickness, embedded in carbon-enriched austenite. Unlike many methods for the production of nanostructured metals, it becomes possible to create components that are large in all three dimensions, with uniform properties throughout. The fundamental mechanisms behind this nanostructured steel are now fairly well-understood, along with the factors determining its strength, ductility and fracture toughness [20].

Nevertheless, there are difficulties which prevent the wider exploitation of the nanostructure. The large carbon concentration of the steel (about 1 wt%) prevents it from being welded because of the brittle, untempered martensite induced in the heat-affected zone of the joint [21, 22]. This dramatically reduces the utility of the steel to objects such as shafts, bearings and armour. The second difficulty is the poor impact toughness of just 5 J of absorbed energy at 20°C, in spite of the more than acceptable fracture toughness ($K_{IC}$) at a strength of more than 2 GPa.

Weldability in the context of strong steels can in principle be achieved by reducing the carbon concentration to less than $\approx 0.3$ wt% [23] but this would compromise the strength if the structure remains bainitic [24, 25]. A martensitic structure can achieve the required strength at that concentration of carbon, but the toughness would not then be impressive. And toughness is essential for weldability.

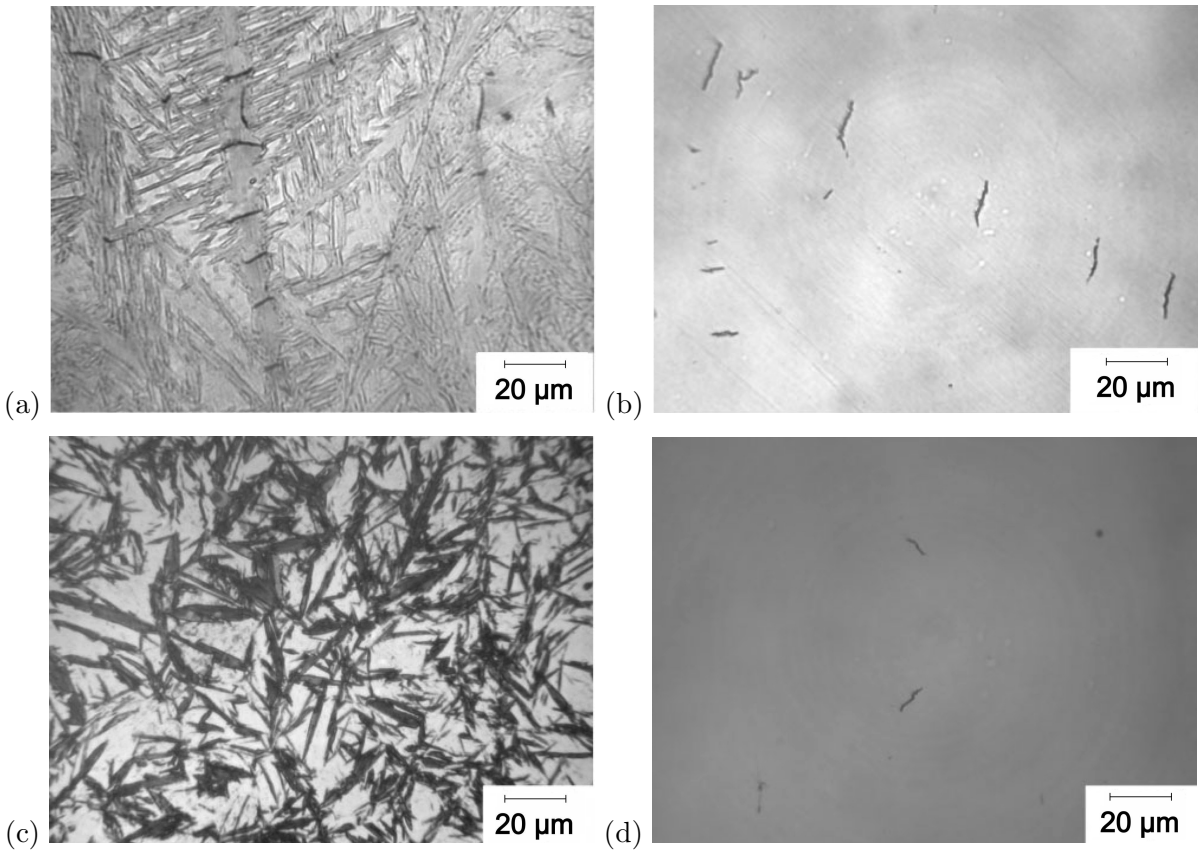


**Figure 4.** Microscopic cracking of martensite plates. (a,b) Etched and unetched samples respectively, showing martensite plates in austenite with a grain size (mean lineal intercept) of 410±53 µm. (c,d) Etched and unetched samples respectively, showing martensite plates in austenite with a grain size (mean lineal intercept) of 65±12 µm [26].

The general impression that high-carbon martensite is brittle may not be correct. Untempered high-carbon martensite is induced during the deformation of TRIP-assisted steels, and yet, they are formable. The induced-martensite does not crack even at large plastic strains. In fact, it is the large blocks of martensite that have been demonstrated to be brittle [27, 28]. A study of the microscopic cracking of martensite in a 1 wt% carbon alloy-steel has shown that the tendency for cracking is sensitive to the absolute size of martensite plates [26]. This is because load transfer onto the hard martensite becomes difficult as the scale of the martensite decreases. figure 4 illustrates the experiments in which the size of the martensite plates was controlled

by altering the austenite grain size. There are two key observations, first, that the extent of cracking diminishes as the austenite grain size (and hence martensite plate size) is reduced. Secondly, the spacing of cracks in a fragmented plate is approximately constant and corresponds to a stress-transfer length of about 10 µm. Therefore, reducing the austenite grain size to a number less than 10 µm should dramatically increase the fracture toughness.

The approach is presented in figure 5, with the aim of generating fine martensite by rendering the austenite into a pancaked state using a particularly low finish-rolling temperature, combined with vanadium microalloying to ensure that the austenite, and its deformation defects, do not recover or recrystallise before martensitic transformation.

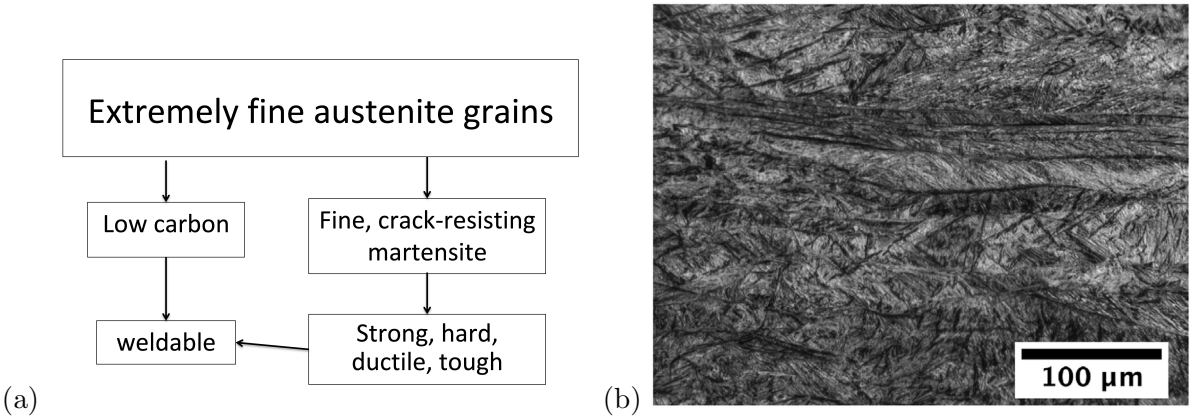


**Figure 5.** (a) Methodology for achieving tough and strong martensite. (b) Pancaked prior austenite grain structure, also containing deformation bands, after Chintha et al. [29].

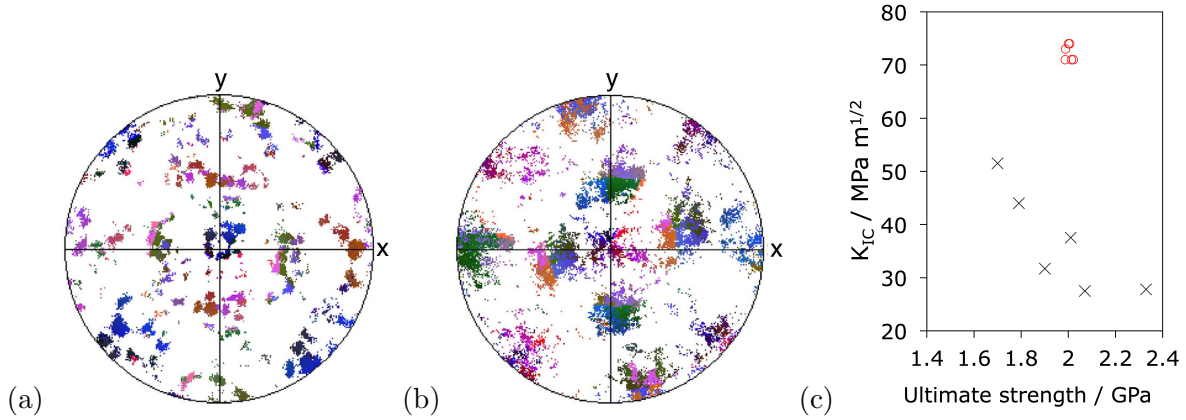


**Figure 6.** Stereographic projections relative to sample axes, showing martensite $\{100\}_{\alpha'}$ poles. (a) Martensite poles from a single, undeformed, prior austenite grain. (b) Martensite poles from a severely deformed, pancaked, prior austenite grain, showing an enormous spread of orientations [29]. (c) Mechanical properties of new steel (red circles - data courtesy of Dr S. Kundu, Tata Steel India) contrasted against a bulk nanostructured bainitic steel [30].

It is established that a refinement of the "crystallographic grain size", i.e., the size over which crystals are coherent, improves toughness by providing frequent intersections where a propagating cleavage crack must change orientation or adopt a complex topology as it traverses

the coherent space [31–36]. The caveat is that the material must not be so brittle that boundaries are of little consequence [33]. The boundaries themselves do not contribute much to the cleavage resistance [37]. figure 6 shows $\{100\}_{\alpha'}$ martensite pole figures, each taken from a single prior-austenite grain, in both the deformed-austenitic and undeformed-austenitic states. The deformation of the austenite results in a huge spread in the orientations of the martensite plates that form subsequently, in contrast to the martensite that grows from undeformed austenite. This crystallographic *chaos* in the former case is because there is a spread of orientations within a defect-rich austenite grain. This, combined with the fine scale of the martensite plates, causes a large increase in the toughness of the steel; comparative data are presented in figure 6c.

To paraphrase, untempered martensite in Fe-C need not be brittle if its length scale is reduced and if the plates are crystallographically dispersed to induce complex cleavage.

## 4. Limit of detection

It often is taken for granted the austenite to martensite transformation occurs at a unique temperature, designated $M_{\rm S}$. The fact that $M_{\rm S}$ depends on the sensitivity of the measuring technique is neglected in reaching this conclusion. Acoustic emission measurements record a greater $M_{\rm S}$ than the monitoring of electrical resistivity [38]. The martensite-start temperature depends also on the austenite grain size (figure 7) but curiously, this is a manifestation of the sensitivity described above. The size of the largest martensite plate that can form is related to the austenite grain size ($\overline{L}_\gamma$). The thickness to length ratio of a martensite plate is constant as the strain energy due to the shape deformation [39] balances with the chemical driving force. Therefore, the volume per plate of martensite will increase with $\overline{L}_\gamma$. If the same number of plates form in a large and small austenite grain, the latter would be more difficult to detect because the absolute volume of martensite would be smaller. Based on this concept, the classical Koistinen and Marburger equation [40]:

$$1 - V_{\rm V}^{\alpha'} = \exp\{-\beta[T - M_{\rm S}]\} \tag{3}$$

where $\beta$ is a constant, becomes [41]:

$$M_{\rm S}^{\circ} - M_{\rm S} = \frac{1}{b}\ln\left[\frac{1}{\overline{L}_\gamma^3}\left\{\exp\left(-\frac{\ln(1 - V_V^{\alpha'})}{m}\right) - 1\right\} + 1\right] \tag{4}$$

where $b = 0.2689$, $\overline{L}_\gamma$ is in mm, $m = 0.05$ is the aspect ratio of martensite plates, and $M_{\rm S}$ is defined when a fraction $V_{\rm V}^{\alpha'} = 0.01$ of martensite is obtained. The term $M_{\rm S}^o$ is defined as a fundamental martensite-start temperature for an austenite grain size that is so large that the formation of just one martensite plate is detectable using routine methods. It is given by the point where $\Delta G^{\gamma\to\alpha} = 700\,{\rm J\,mol^{-1}}$, i.e. the stored energy of martensite due to the shape deformation and twin interfaces. $M_{\rm S}^o$ is therefore purely a thermodynamic quantity with no consideration given to kinetic effects. figure 7 shows that the effect becomes insignificant beyond about 40μm so in conventional experiments, the issue is likely lost in the $\pm 20\,^{\circ}$C noise present in typical experimental data [42].

## 5. Steep diffusion gradients

It could be argued that the interpretation of growth rate data on the formation of ferrite in steels, is in a state of crisis. There is a failure to account for the limitations of experimental techniques and difficulties with the theory of diffusion-controlled growth in multicomponent steels. One might be forgiven in deducing from the published literature that whenever there is a gap between theory and experiment, it is explained by appealing to free energy dissipations that have little in the way of supporting evidence [43].

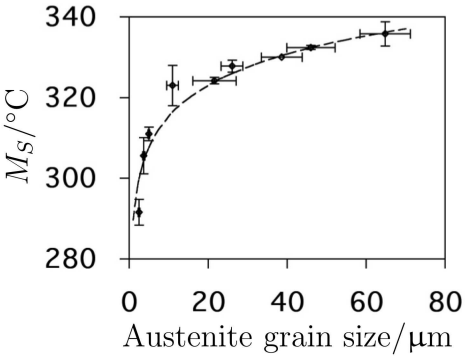


**Figure 7.** Measured variation in the martensite–start temperature as a function of austenite grain size, determined from dilatometric data (after Yang et al. [41]). This entire variation can be explained by the resolution of the experimental technique coupled with the spatial constraints that exist during the formation of elastically accommodated martensite plates in a given size of austenite grain.

A particular difficulty is that kinetic models for the growth of ferrite in multicomponent steels at large supersaturations leads to extremely steep gradients of concentration, recognised to be unrealistic in the original theoretical work by Coates [44]. There are publications in which the diffusion spike within the austenite, required to maintain local equilibrium at the $\alpha/\gamma$ interface while permitting the fluxes of substitutional and interstitials to keep pace, is just 0.03-0.003 nm in width. This clearly is physically impossible.

There are additional terms in diffusion theory when gradients are steep [reviewed by Hilliard in 45], which ensure, for example, that the composition waves that develop during spinodal decomposition have finite wavelengths. Whereas a homogeneous chemical solution of composition $\overline{c}$ can be ascribed a particular free energy per atom of $g\{\overline{c}\}$, that of a heterogeneous solution containing concentration gradients, $g_{\rm ih}$ is expressed as a multivariate Taylor expansion:

$$\begin{aligned} g_{\rm ih}\{a,b,\ldots\} &= g\{\overline{c}\} + a\frac{\partial g}{\partial a} + b\frac{\partial g}{\partial b} + \ldots \\ &\quad + \frac{1}{2}\left[a^2\frac{\partial^2 g}{\partial a^2} + b^2\frac{\partial^2 g}{\partial b^2} + 2ab\frac{\partial^2 g}{\partial a\,\partial b} + \ldots\right] + \ldots \end{aligned} \tag{5}$$

in which the variables, $a, b, \ldots$ in our context are the spatial composition derivatives ($\mathrm{d}c/\mathrm{d}z$, $\mathrm{d}^2c/\mathrm{d}z^2$, etc). After considerable mathematical manipulation [45] this becomes

$$g_{\rm ih} = \int\left[g\{\overline{c}\} + v_{\rm a}^3\kappa(\nabla c)^2\right]dV \tag{6}$$

where $v_{\rm a}$ is the volume per atom and $\kappa$ is known as the gradient energy coefficient. Gradients of concentration lead to an increase in the free energy, so that the formation of steep gradients will in general be opposed. The application of this to ferrite growth is described in detail elsewhere [43], but figure 8 shows that the cost of the steep gradient becomes overwhelming at the sort of concentration spikes typical in the analysis of ferrite growth involving the negligible partitioning of substitutional solutes. This mode of growth is physically unrealistic, the alternative being that local equilibrium breaks down. In summary, any process that involves concentration profiles over very short distances must account for the gradient energy term. This includes, for example, models of solute drag that often are called upon to wile away discrepancies between experiments and theory.

## 6. Strength

The strength of crystals increases as they are made smaller because the chances of avoiding defects become greater as the volume of the sample decreases. Imperfections in the form of

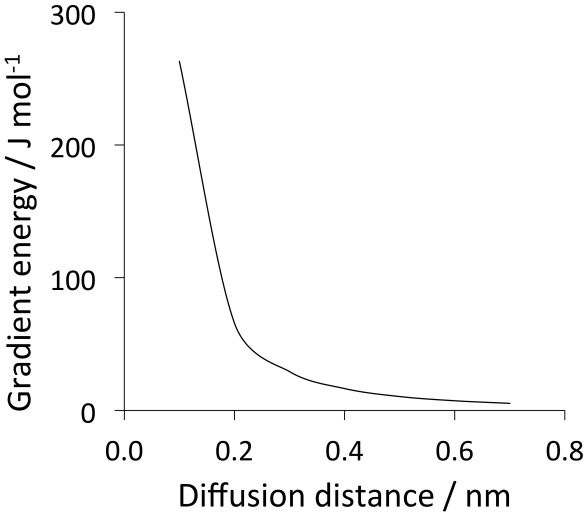


**Figure 8.** Estimate of the penalty on free energy due to the gradient of concentration in the austenite ahead of the $\alpha/\gamma$ interface. The diffusion distance in many calculations of growth with local equilibrium are much less than 0.01 nm, in which case, the penalty would be intolerable. This penalty essentially rules out any mechanism of diffusion-controlled growth that necessitates the existence of steep gradients, a case in hand being the so-called negligible-partitioning local equilibrium mode.

dislocations are able to facilitate shear at much lower stresses than would be the case if whole planes of atoms had to collectively slide across each other.

In an ideal, defect-crystal, the tensile strength $\sigma_t \simeq 0.1E$ where $E$ is the Young's modulus. The corresponding ideal shear-strength is $\sigma_s \simeq b\mu/2\pi a$, where $\mu$ is the shear modulus, $b$ is a repeat period along the displacement direction and $a$ is the spacing of the slip planes. For ferritic iron, $\mu = 80.65$ GPa and $E \simeq 208.2$ GPa. It follows that the ideal values of tensile and shear strength should be about 21 and 11 GPa, respectively. Strengths approaching the theoretical values were achieved by Brenner as long ago as 1956 (figure 9a) during the testing of single-crystals of iron with diameters less than 2 µm.

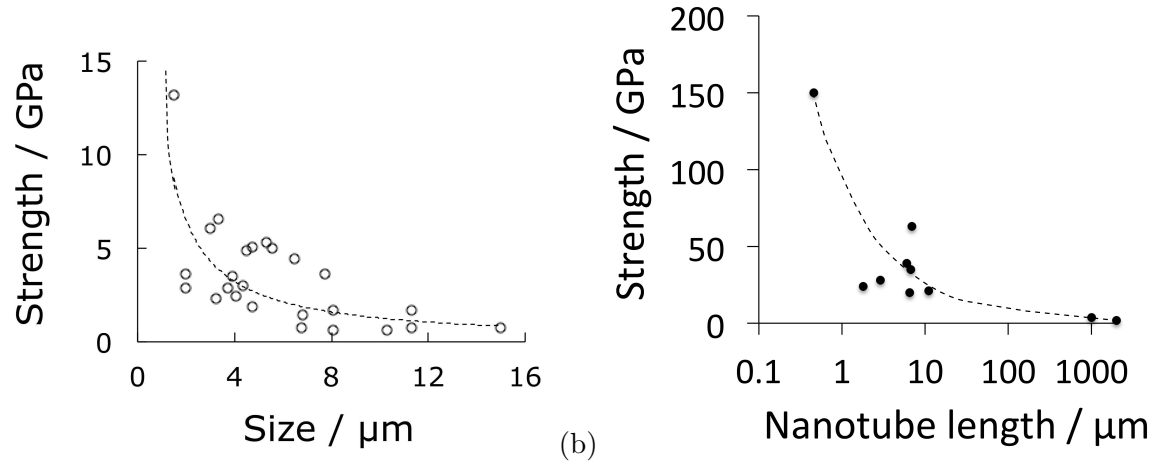


**Figure 9.** (a) The tensile strength of whiskers of iron [46, 47]. (b) Variation in the strength of carbon nanotubes as a function of length. Data collated from [48–50].

The experiments showed that the strength decreased sharply as the dimensions of the test-sample were increased (figure 9a), because the chances of finding defects increase as the sample gets bigger. It is therefore not wise to rely on perfection as a method of designing strong materials.

Carbon nanotubes can be imagined to be constructed from sheets of graphene consisting of $sp^2$ carbon arranged in a two-dimensional hexagonal lattice. The breaking strength of such a tube has been estimated to be an extraordinary 130 GPa, leading to many exaggerated comparisons against steel. However, this is the strength of an invisibly small nanotube. Larger tubes will contain defects that lead to a gross deterioration of strength, rather like the behaviour of single-crystals of iron. Some of these defects will be there at equilibrium and hence are unavoidable. For example, it is known that metals contain an *equilibrium* concentration of vacancies. The enthalpy change associated with the formation of a vacancy opposes its existence, whereas the change in configurational entropy due to the formation of a vacancy favours its formation.

The total change in free energy on forming $n$ vacancies in a crystal is given by [51]:

$$\Delta G = n\Delta g - kT[(N+n)\ln\{N+n\} - N\ln\{N\} - n\ln\{n\}], \tag{7}$$

where $k$ is the Boltzmann constant, $T$ is the absolute temperature, $N$ is the number of atoms, $\Delta g = \Delta h - T\Delta s$, $\Delta h$ is the enthalpy of formation of one vacancy and $\Delta s$ is the entropy of formation of a vacancy excluding any contribution from configurational entropy, which is the second term in the equation. The equilibrium mole fraction of vacancies ($x$) is obtained by writing $\partial\Delta G/\partial n = 0$ giving:

$$x = n/N \simeq \exp\{-\Delta g/kT\}. \tag{8}$$

On this basis, taking the energy of a vacancy in a nanotube as 7 eV, and setting $T$ to be the manufacturing temperature of the tubes (2000-4000 K), it is possible to show that a carbon nanotube strand appropriate for a space elevator, weighing 5000 kg, would contain approximately $10^{10}$-$10^{20}$ defects. In fact, we have the less than surprising result the strength collapses as the length of the tube increases figure 9b. Systems which rely on perfection in order to achieve strength necessarily fail on scaling to engineering dimensions. Indeed, there is no carbon tube which can match the strength of iron beyond a scale of 2 mm. These considerations apply also to graphene sheets.

Graphene has been claimed to be between 100-300 times stronger than steel. Lee and co-workers determined the strength of a monolayer of graphene about 1 μm in diameter by a nanoindentation method [52]. They measured the intrinsic breaking strength of the perfect layer as 42 N m$^{-1}$ and converted this into a strength of 130 GPa, the same value as reported for carbon nanotubes [53], which may not be surprising given that the data are in both cases for carbon-carbon bonds in perfect samples. Suppose that 130 GPa represents the true strength of two-dimensional graphene. Brenner [46] has measured the tensile strength of a 1.6 μm whisker to be 13.4 GPa so the intrinsic tensile strength of iron, along its weakest crystallographic direction is likely to be 14.2 GPa [54]. If follows that that pristine graphene is at best about 9 times stronger than steel. When scaled to sizes greater than the micrometre dimensions, it is likely to suffer the same fate as carbon nanotubes, i.e. lose its integrity. More detail in [55].

## 7. Summary

The study of scaling effects presents a fertile ground for revealing research, but it has only been possible to describe a few of the effects here. A few further examples in the context of steels, not described here but available in the open literature, are as follows:

- small concentrations of stainless steel nanoparticles in fluids disproportionately influencing their thermal conductivity [56];
- comparison of carbon concentration analysis using the atom probe, transmission electron microscopy and X-ray diffraction [57];
- the thermodynamics of the evolution of a solid solution beginning with large particles that are forced to mix at ever decreasing sizes by mechanical alloying [58].

A particular difficulty that has yet to addressed quantitatively, is how promising studies based on the characterisation of small laboratory samples (60 g-100 kg) can be scaled to much larger commercially viable quantities for component level testing. This is an Achilles heal of many alloy design programmes.

**Acknowledgments:** Many congratulations to Risø DTU National Laboratories on this 40th anniversary of the international symposia that have contributed regularly to our understanding of materials.

## References

[1] Hehemann R F 1970 The bainite transformation *Phase Transformations* ed Aaronson H I and Zackay V F (Materials Park, Ohio, USA: American Society of Materials) pp 397–432

[2] Ko T and Cottrell S A 1952 *Journal of the Iron and Steel Institute* **172** 307–313

[3] Srinivasan G R and Wayman C M 1968 *Acta Metallurgica* **16** 621–636

[4] Swallow E and Bhadeshia H K D H 1996 *Materials Science and Technology* **12** 121–125

[5] Peet M and Bhadeshia H K D H 2011 *Metallurgical & Materials Transactions A* **42** 3344–3348

[6] Bhadeshia H K D H and Edmonds D V 1979 *Metallurgical Transactions A* **10A** 895–907

[7] Chatterjee S, Wang H S, Yang J R and Bhadeshia H K D H 2006 *Materials Science and Technology* **22** 641–644

[8] Machlin E S and Cohen M 1951 *Trans. Metall. Soc. AIME* **191** 746–754

[9] Fiedler H C, Averbach B L and Cohen M 1955 *Transactions of the American Society for Metals* **47** 267–290

[10] Bhadeshia H K D H 1978 *Theory and Significance of Retained Austenite in Steels* Ph.D. thesis University of Cambridge Cambridge, U. K.

[11] Mandelbrot B B 1983 *The fractal geometry of nature* (New York, USA: W. H. Freeman)

[12] Turnbull A and Hutchings R B 1994 *Materials Science & Engineering A* **177** 161–171

[13] Bhadeshia H K D H 2016 *ISIJ International* **56** 24–36

[14] Knott J F 1981 *Fundamentals of Fracture Mechanics* (London: Butterworths)

[15] Song E J, Suh D W and Bhadeshia H K D H 2013 *Computational Materials Science* **79** 36–44

[16] Kang Y and Bhadeshia H K D H 2006 *Materials Science and Technology* **22** 645–652

[17] Brown P M and Baxter D P 2004 Hyper-strength bainitic steels *Materials Science and Technology 2004* (Warrendale, Pennsylvania, USA: TMS) pp 433–438

[18] Secretary of State for Defence, Bhadeshia H K D H, Mateo C and Brown P 2010 Bainite steel and methods of manufacture thereof Tech. Rep. GB2462197 Intellectual Property Office London, U.K.

[19] Bhadeshia H K D H 2010 *Proceedings of the Royal Society of London A* **466** 3–18

[20] Bhadeshia H K D H 2013 *Science and Technology of Advanced Materials* **14** 014202

[21] Hong S G, Cho M H and Lee J S 2010 Effect of post weld rapid heat treatment on microstructural evolution in high-carbon bainitic steel welds *63rd Annual Assembly and International Conference of the International Institute of Welding* vol AWST-10/99 (France: International Institute of Welding) pp 47–51

[22] Fang K, Yang J, Zhao D, Song K, Yan Z and Fang H 2012 *Advanced Materials Research* **482-484** 2405–2408

[23] Lancaster J F 1970 *The metallurgy of welding brazing and soldering* (London, U.K.: George Allen and Unwin Ltd, eds C. R. Tottle and J. C. Wright)

[24] Pickering F B 1978 *Physical Metallurgy and the Design of Steels* (Essex, U.K.: Applied Science Publishers, page 104)

[25] Khare S, Lee K Y and Bhadeshia H K D H 2010 *Metallurgical & Materials Transactions A* **41A** 922–928

[26] Chatterjee S and Bhadeshia H K D H 2006 *Materials Science and Technology* **22** 645–649

[27] Bhadeshia H K D H and Edmonds D V 1983 *Metal Science* **17** 411–419

[28] Bhadeshia H K D H and Edmonds D V 1983 *Metal Science* **17** 420–425

[29] Chintha A R, Peet M, Kundu S, Bhadeshia H K D H, Valtonen K and Kuokkala V T 2019 *Wear* **428-429** 430–437

[30] Bhadeshia H K D H 2015 *Bainite in steels: theory and practice* 3rd ed (Leeds, U.K.: Maney Publishing)

[31] Gourgues A F, Flower H M and Lindley T C 2000 *Materials Science and Technology* **16** 26–40

[32] Lambert-Perlade A 2001 *Rupture par clivage de microstructures d'aciers bainitiques obtenues en conditions de soudage* Ph.D. thesis Ecole de Mines de Paris Paris, France

[33] Qiao Y and Argon A S 2003 *Mechanics of Materials* **35** 313–331

[34] Nohava J, Hausild P, Karlik M and Bompard P 2003 *Materials Characterization* **49** 211–217

[35] Lambert-Perlade A, Gourgues A F and Pineau A 2004 *Acta Materialia* **52** 2337–2348

[36] Lambert-Perlade A, Gourgues A F, Besson J, Sturel T and Pineau A 2004 *Metallurgical & Materials Transactions A* **35** 1039–1053

[37] Qiao R and Argon A S 2003 *Mechanics of Materials* **35** 129–154

[38] Olson G B, Tsuzaki K and Cohen M 1987 *Mat. Res. Soc. Symposium Proc.* **57** 129–148

[39] Christian J W 1958 *Acta Metallurgica* **6** 377–379

[40] Koistinen D P and Marburger R E 1959 *Acta Metallurgica* **7** 59–60

[41] Yang H S and Bhadeshia H K D H 2009 *Scripta Materialia* **60** 493–495

[42] Yang H S and Bhadeshia H K D H 2007 *Materials Science and Technology* **23** 556–560

[43] Bhadeshia H K D H 2016 *Current Opinion in Solid State and Materials Science* **20** 396–400

[44] Coates D E 1973 *Metallurgical Transactions* **4** 395–396

[45] Hilliard J E 1970 Spinodal decomposition *Phase Transformations* ed Zackay V F and Aaronson H I (Metals Park, Ohio, USA: ASM International) pp 497–560

[46] Brenner S S 1956 *Journal of Applied Physics* **27** 1484–1491

[47] Brenner S S 1956 *Acta Metallurgica* **4** 62–74

[48] Yu M F, Lourie O, Dyer M J, Moloni K, Kelly T F and Rouff R S 2000 *Science* **287** 637–640

[49] Xie S, Li W, Pan Z, Chang B and Sun L 2000 *Journal of Physics and Chemistry of Solids* **61** 1153–1158

[50] Pan Z W, Xie S S, Lu L, Chang B H, Sun L F, Zhou W Y, Wang G and Zhang D L 1999 *Applied Physics Letters* **74** 3152–3154

[51] Christian J W 2003 *Theory of Transformations in Metals and Alloys, Part I* 3rd ed (Oxford, U. K.: Pergamon Press)

[52] Lee C, Wei X, Kysar J W and Hone J 2008 *Science* **321** 385–388

[53] Yakobson B I and Smalley R E 1997 *American Scientist* **85** 324–337

[54] Clatterbuck D M, Chrzan D C and J W Morris Jr 2002 *Philosophical Magazine Letters* **82** 141–147

[55] Bhadeshia H K D H and Honeycombe R W K 2017 *Steels: Microstructure and Properties* 4th ed (Elsevier)

[56] Song Y Y, Bhadeshia H K D H and Suh D W 2015 *Powder Technology* **272** 34–44

[57] Bhadeshia H K D H 2015 *Materials Science and Technology* **31** 758–763

[58] Badmos A Y and Bhadeshia H K D H 2000 *Metallurgical & Materials Transactions A* **28** 2189–2193